Incipient Fluidization Condition for a Centrifugal Fluidized Bed

L. T. FAN, C. C. . CHANG,
and
Y. S. YU

Department of Chemical Engineering
Kansas State University
Manhattan, KS 66506

and

TERUO TAKAHASHI and
ZENNOSUKE TANAKA

Department of Industrial Chemistry
Faculty of Engineering, Okayama University
3-1-1, Tsushima-naka, Okayama, Japan 700

A model has been proposed for the condition of incipient fluidization in a centrifugal fluidized bed. The model is based on the balance between the overall forces, including the centrifugal and fluid frictional forces, exerted on the fluidized particles and the overall effective weight of the particles. Equations have been derived from the model for predicting the critical fluidizing velocity and the maximum pressure differential (or pressure drop) through the centrifugal bed. A series of experiments was carried out with different solid particles, bed rotational speeds, and bed heights. The resultant data for the critical fluidizing velocity and the maximum pressure drop of the bed indicate that the proposed model is valid and the derived equations are of practical use.

SCOPE

Fluidized beds have many advantages as gas-solid contactors. For example, mass and heat are transferred rapidly in the beds and, therefore, temperature and concentration can be maintained uniformly throughout the beds. In addition, solids may be added or removed during operation, which renders continuous operation possible. Thus fluidization technology has been employed extensively in process industries. However, the application of a fluidized bed can be limited, sometimes, by the necessity of pumping a large volume of fluidizing medium through it. This can cause violent slugging or lifting of the fluidized particles out of the bed, thereby creating difficulties in using fluidized beds in industrial applications such as coal combustion, filtration of dusty air, flue gas desulfurization, and solids drying. Recently, the use of centrifugal fluidized beds has received much attention for application in these areas (see, e.g., Gal et al., 1982; Kroger et al., 1979, 1980; Lazar and Farkas, 1971; Farkas et al., 1969). A review of early works is given by Fan (1978).

In a centrifugal fluidized bed, particles are fluidized in the centrifugal field. The bed usually consists of a cylindrical basket that rotates about its axis of symmetry; the rotation of the axis causes the particles in the basket to form an annular region at the circumference of the basket. Fluid is injected inward through the porous surface of the basket wall, and the particles begin to fluidize when the force exerted by the fluidizing medium becomes equal to the effective weight of particles in the centrifugal field (Takahashi et al., 1984).

Features of the centrifugal fluidized bed, especially its advantages over the columnar fluidized bed in gravitational field, are discussed below.

1. The centrifugal fluidized bed can be operated in much wider ranges of conditions than the columnar fluidized bed. In the centrifugal fluidized bed, radial acceleration can be enhanced over the gravitational acceleration, g, by changing the rotational speed of the basket that permits a much larger flow rate per unit area of the distributor than is possible in the columnar fluidized bed, which operates only against the force of gravity.
2. The centrifugal fluidized bed can be used for a variety of process operations in systems outside the gravitational field or in systems in rocking motion, where it is impossible or difficult to employ the columnar fluidized bed. Examples of such systems are spacecrafts, ships, trains, and cars.
3. The centrifugal fluidized bed is easier to control than the columnar fluidized bed; the rotational speed of the basket can be altered so that the particles will fluidize at a desired gas flow rate.
4. When used as a filter, the centrifugal fluidized bed has a higher efficiency and capacity than the columnar fluidized bed. If supplied to the columnar fluidized bed at a velocity higher than the minimum fluidization velocity, dusty gas to be filtered bypasses the bed in the form of bubbles; this results in poor collection efficiency. The drag force of the gas acting on the solid particles in the centrifugal fluidized bed is balanced by the centrifugal force, which is greater than the gravitational force; this leads to the decrease in bubble formation and the consequent increase in filtration efficiency.
5. The space requirement of the centrifugal fluidized bed is much smaller than that of the columnar fluidized bed because of its small distributor surface area and cylindrical geometry.

Different views exist on the incipient fluidization of a centrifugal bed. Gelperin et al. (1964) have extended a simple cor-

relation for predicting the critical fluidization velocity of small particles in the columnar fluidized bed to the centrifugal bed. Demircan et al. (1978) have modified an available correlation (Wen and Yu, 1966) for the onset velocity of fluidization to include the critical fluidization velocity for the centrifugal fluidized bed. Levy et al. (1978) and Kroger et al. (1979) have proposed a mechanistic model to describe the relationship between the critical fluidization velocity and the maximum pressure drop in the centrifugal fluidized bed. Their model considers that when the pressure drop in the centrifugal bed is equal to the effective weight of the solid particles acting on the outside surface of the basket wall, the particles begin to fluidize. All of them have either failed to take into consideration the curvature effect of a cylindrical bed or made simplifying assumptions that may result in appreciable deviations in predicting the minimum fluidization velocity or the maximum pressure drop; in other words, these models appear to represent approximations useful for gross estimation.

The objectives of this work are to propose a fairly general and rigorous mechanistic model for the condition of incipient fluidization in the centrifugal bed, to derive equations for predicting the critical fluidizing velocity, u_{oc}, and the maximum pressure differential, ΔP_{max}, and to verify these equations experimentally.

CONCLUSIONS AND SIGNIFICANCE

A fairly general and rigorous mechanistic model has been proposed for the condition of incipient fluidization in the centrifugal fluidized bed. Equations have been derived from the model for predicting the critical fluidizing velocity, u_{oc}, and the maximum pressure differential, ΔP_{max}, through the centrifugal bed. Each model equation reduces naturally to that of the columnar fluidized bed in the gravitational field when the curvature of a fluidized bed and the centrifugal accelerational force are neglected. The experimental data obtained indicate that the proposed model is valid and the derived equations are of practical use. We should be able to extend the present approach and model to centrifugal fluidized beds involving more than one fluid phase, e.g., liquid and gas phases or liquid and liquid phases, which are important for many processing operations, such as gas absorption, liquid-liquid extraction, and direct-contact heat transfer, all with or without chemical reactions.

THEORETICAL

An exhaustive review of the available information indicates that when the rotational speed of the basket is fixed, the pressure drop through a centrifugal packed bed increases as the fluid velocity increases, and at a certain velocity, the particles at the freeboard surface of the bed will begin to fluidize; at this instance, the pressure differential through the bed reaches the maximum. Thereafter, the pressure differential through the bed declines as the fluid flow continuously increases.

The above observation renders us to postulate that fluidization is initiated when the force exerted by the fluid flowing through the bed is equal to the total effective weight of the particles in the centrifugal bed under the assumption that the radial velocity of the fluid is uniformly distributed on the radial surface of the bed. The pressure drop through a packed bed in the centrifugal bed with a differential radius of dr can be expressed in terms of the sum of the drag force as correlated by Ergun (1952) and the centrifugal and dynamic forces experienced by it. Thus (see Figure 1 and Appendix A)

$$\left.\begin{aligned} \frac{dP}{dr} &= \phi_1 u + \phi_2 u^2 + \rho_f \omega^2 r + \rho_f \frac{u^2}{r} \\ \text{or} \\ \frac{dP}{dr} &= \phi_1 u + \left(\phi_2 + \frac{\rho_f}{r}\right) u^2 + \rho_f \omega^2 r \end{aligned}\right\} \quad (1)$$

where ϕ_1, ϕ_2, and u are defined, respectively, as

$$\phi_1 = \frac{150(1-\epsilon)^2 \mu}{\epsilon^3 (\phi_s d_p)^2} \quad (2)$$

$$\phi_2 = \frac{1.75(1-\epsilon)\rho_f}{\epsilon^3 \phi_s d_p} \quad (3)$$

$$u = |u_r| \quad (4)$$

If the sphericity, ϕ_s, is not obtainable experimentally, a correlation suggested by Wen and Yu (1966) can be used to eliminate it from ϕ_1 and ϕ_2; the correlating equations are

$$\frac{1}{\phi_s \epsilon^3} \cong 14 \quad \text{and} \quad \frac{1-\epsilon}{\phi_s^2 \epsilon^3} \cong 11 \quad (5)$$

Substituting these expressions into the equations of ϕ_1 and ϕ_2 yields, respectively

$$\phi_1 = \frac{1650(1-\epsilon)\mu_f}{d_p^2} \quad (6)$$

$$\phi_2 = \frac{24.5(1-\epsilon)\rho_f}{d_p} \quad (7)$$

The overall pressure differential across the entire bed is obtained by integrating Eq. 1, i.e.

$$\begin{aligned} \Delta P &= \int_{P|_{r_i}}^{P|_{r_o}} dP \\ &= \int_{r_i}^{r_o} \left(\phi_1 u + \phi_2 u^2 + \rho_f \omega^2 r + \rho_f \frac{u^2}{r}\right) dr \end{aligned} \quad (8)$$

where

$$\Delta P \equiv P|_{r_o} - P|_{r_i} = P_{r_o} - P_{r_i} \quad (9)$$

The continuity of fluid requires that

$$u = u_o \frac{r_o}{r} \quad (10)$$

Thus

$$\begin{aligned} \Delta P = \phi_1 u_o r_o \ln \frac{r_o}{r_i} + \phi_2 u_o^2 r_o^2 \left(\frac{1}{r_i} - \frac{1}{r_o}\right) \\ + \frac{\rho_f \omega^2}{2}(r_o^2 - r_i^2) + \frac{\rho_f u_o^2 r_o^2}{2}\left(\frac{1}{r_i^2} - \frac{1}{r_o^2}\right) \end{aligned} \quad (11)$$

Under a steady operating condition, the force acting on the particles in a differential volume in the bed, with a differential

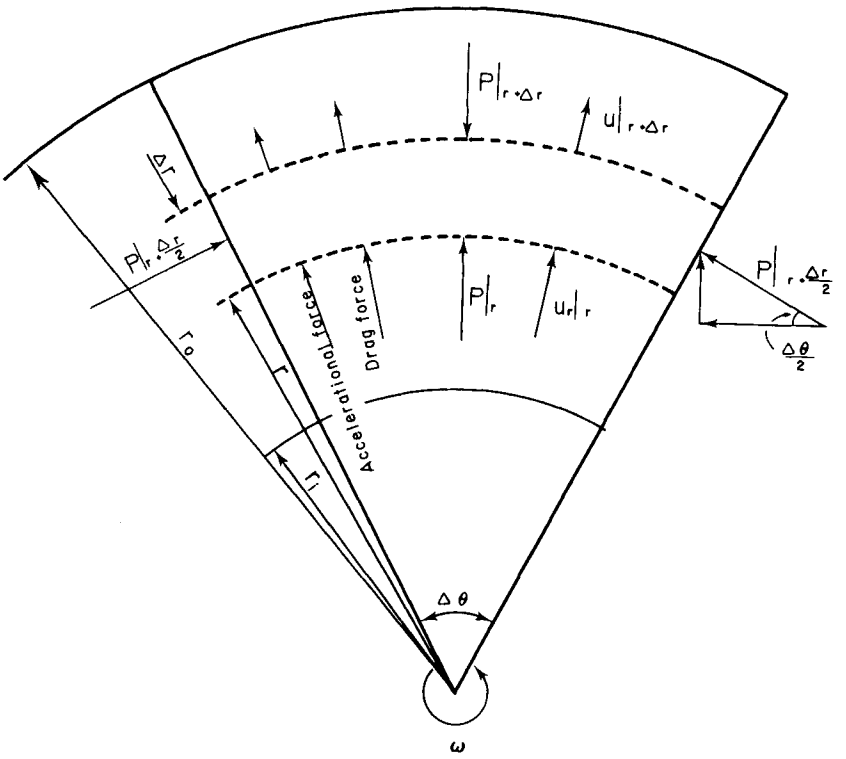

Figure 1. Schematic of a section of the centrifugal fluidized bed.

thickness of dr, is equal to the product of the pressure drop through it, dP, and the radial area, $2\pi rL$, resulting in

$$dF = -2\pi rL(dP)$$
$$= -2\pi rL\left(\phi_1 u + \phi_2 u^2 + \rho_f \omega^2 r + \rho_f \frac{u^2}{r}\right) dr \qquad (12)$$

Thus the overall forces exerted on the particles in the entire bed from r_i to r_o is

$$-F = -\int_0^F dF$$
$$= \int_{r_i}^{r_o} 2\pi rL\left(\phi_1 u + \phi_2 u^2 + \rho_f \omega^2 r + \rho_f \frac{u^2}{r}\right) dr$$
$$= 2\pi L\left[\phi_1 u_o r_o (r_o - r_i) + \phi_2 u_o^2 r_o^2 \ln\frac{r_o}{r_i} + \frac{\rho_f \omega^2}{3}(r_o^3 - r_i^3) + \rho_f u_o^2 r_o^2\left(\frac{1}{r_i} - \frac{1}{r_o}\right)\right] \qquad (13)$$

If the gravitational effect is neglected, the overall effective weight of the particles in the centrifugal bed is

$$G = \int_{r_i}^{r_o} (1-\epsilon)(\rho_s - \rho_f) 2\pi L \omega^2 r^2 dr$$
$$= \frac{2\pi}{3} L\omega^2 (1-\epsilon)(\rho_s - \rho_f)(r_o^3 - r_i^3) \qquad (14)$$

Table 1. List of Available Models in the Centrifugal Fluidized Bed

Model	u_{oc}	ΔP_{max}
Demircan et al. (1978)	$Re = \frac{d_p u_{oc}\rho_f}{\mu_f} = [(33.7)^2 + 0.0408\,Ga]^{1/2} - 33.7$ $Ga = \frac{\rho_f(\rho_s - \rho_f)\omega^2 r_o d_p^3}{\mu^2}$	$\Delta P_{max} = \rho_B g' h$ $= [(1-\epsilon)\rho_s + \epsilon\rho_f]\omega^2 r_o (r_o - r_i)$
Levy et al. (1978)	$\frac{150(1-\epsilon)}{\epsilon^3\phi_s} Re + \frac{1.75}{\phi_s d_p} Re^2 = Ga$	$\Delta P_{max} = \phi_1 u_{oc} r_o \ln\frac{r_o}{r_i} + \phi_2 u_{oc}^2 r_o^2\left(\frac{1}{r_i} - \frac{1}{r_o}\right)$
Present (1985)	$\left[\phi_2 r_o^2 \ln\frac{r_o}{r_i} + \rho_f r_o^2\left(\frac{1}{r_i} - \frac{1}{r_o}\right)\right] u_{oc}^2 + \phi_1 r_o (r_o - r_i) u_{oc}$ $- \frac{\omega^2}{3}[(1-\epsilon)(\rho_s - \rho_f) - \rho_f](r_o^3 - r_i^3) = 0$	$\Delta P_{max} = \phi_1 u_{oc} r_o \ln\frac{r_o}{r_i} + \phi_2 u_{oc}^2 r_o^2\left(\frac{1}{r_i} - \frac{1}{r_o}\right)$ $+ \frac{\rho_f \omega^2}{2}(r_o^2 - r_i^2)$ $+ \frac{\rho_f u_{oc}^2 r_o^2}{2}\left(\frac{1}{r_i^2} - \frac{1}{r_o^2}\right)$

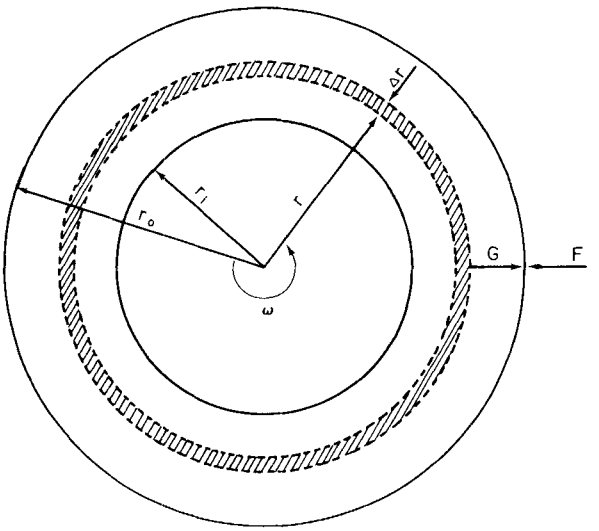

Figure 2. Force balance around fluid in the centrifugal fluidized bed.

According to the present model, the particles near the outside of the freeboard of the bed begin to fluidize when (see Figure 2)

$$F + G = 0 \quad \text{or} \quad G = -F \tag{15}$$

Therefore, the critical fluidization velocity, u_{oc}, can be calculated by equating Eq. 12 and 13; this yields

$$\left[\phi_2 r_o^2 \ln\frac{r_o}{r_i} + \rho_f r_o^2\left(\frac{1}{r_i} - \frac{1}{r_o}\right)\right] u_{oc}^2 + \phi_1 r_o(r_o - r_i)u_{oc} - \frac{\omega^2}{3}[(1-\epsilon)(\rho_s - \rho_f) - \rho_f](r_o^3 - r_i^3) = 0 \tag{16}$$

or

$$Au_{oc}^2 + Bu_{oc} + C = 0 \tag{17}$$

which, in turn, results in

$$u_{oc} = \frac{-B + \sqrt{B^2 - 4AC}}{2A} \tag{18}$$

where

$$A = \phi_2 r_o^2 \ln\frac{r_o}{r_i} + \rho_f r_o^2\left(\frac{1}{r_i} - \frac{1}{r_o}\right) \tag{19}$$

$$B = \phi_1 r_o(r_o - r_i) \tag{20}$$

$$C = -\frac{\omega^2}{3}[(1-\epsilon)(\rho_s - \rho_f) - \rho_f](r_o^3 - r_i^3) \tag{21}$$

By replacing u_o in Eq. 11 with u_{oc}, the maximum pressure differential through the centrifugal bed, ΔP_{max}, is calculated as follows:

$$\Delta P_{max} = \phi_1 u_{oc} r_o \ln\frac{r_o}{r_i} + \phi_2 u_{oc}^2 r_o^2\left(\frac{1}{r_i} - \frac{1}{r_o}\right) + \frac{\rho_f \omega^2}{2}(r_o^2 - r_i^2) + \frac{\rho_f u_{oc}^2 r_o^2}{2}\left(\frac{1}{r_i^2} - \frac{1}{r_o^2}\right) \tag{22}$$

Table 1 lists the available models for calculating the maximum pressure differential, ΔP_{max}, and the critical fluidizing velocity, u_{oc}, in the centrifugal fluidized bed. Note that the present model reduces to the model by Levy et al. (1978) and the model for the columnar fluidized bed in the gravitational field as illustrated below.

Dividing Eq. 16 by $(r_o - r_i)$ yields

$$\phi_1 r_o u_{oc} + \phi_2 r_o^2 \frac{\ln\frac{r_o}{r_i}}{(r_o - r_i)} u_{oc}^2 + \rho_f u_{oc}^2 \frac{r_o}{r_i} = \frac{1}{3}[(1-\epsilon)(\rho_s - \rho_f) - \rho_f]\omega^2(r_o^2 + r_i r_o + r_i^2) \tag{23}$$

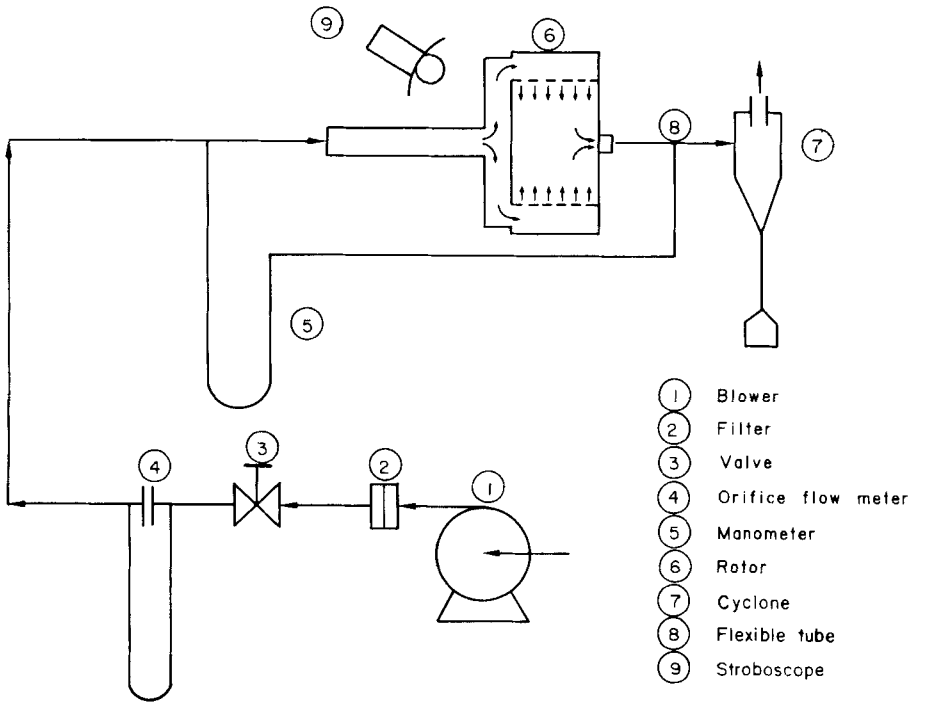

Figure 3. Arrangement of the experimental apparatus.

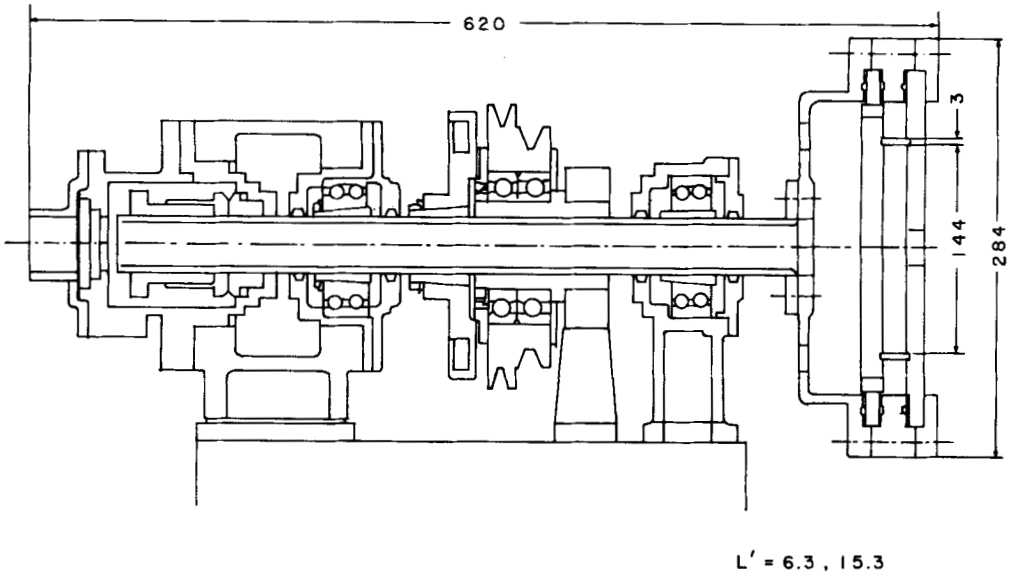

Figure 4. Design of the centrifugal fluidized bed.

When the thickness of the fluidized bed becomes small, i.e., $r_i \to r_o$, we have

$$\lim_{r_i \to r_o} \frac{\ln \frac{r_o}{r_i}}{(r_o - r_i)} = \frac{1}{r_o}$$

and thus

$$\phi_1 u_{oc} + \phi_2 u_{oc}^2 + \frac{\rho_f}{r_o} u_{oc}^2 = (1 - \epsilon)(\rho_s - \rho_f)\omega^2 r_o - \rho_f \omega^2 r_o \quad (24)$$

If the curvature effect is assumed negligible, the continuity equation of fluid gives

TABLE 2. PHYSICAL PROPERTIES OF PARTICLES EMPLOYED IN THE EXPERIMENTS

	Particle Diameter d_p, μm	Particle Density ρ_s, kg/m³	Bulk Density ρ_b, kg/m³
Glass beads	63–74	2,410	1293
	88–105	2,450	1373
	125–149	2,490	1392
	74–125	2,410	1395
Sand	149–177	2,670	1438
	210–250	2,670	1426
	297–350	2,700	1414
Magnesia clinker	74–88	3,650	1476
	88–105	3,630	1460
	125–149	3,620	1339

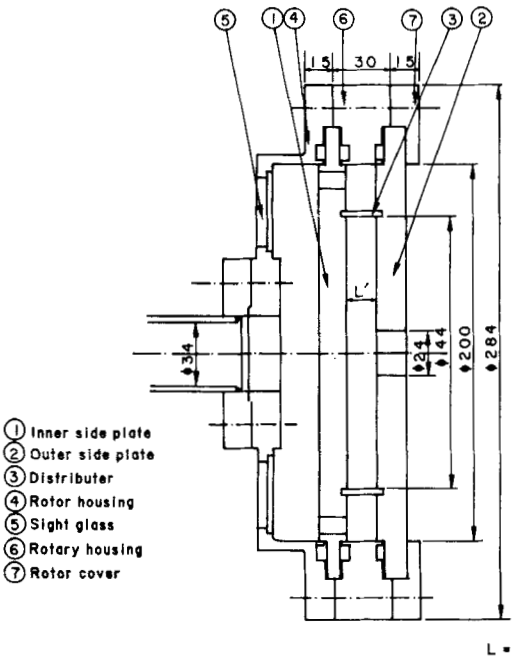

Figure 5. Rotor assembly.

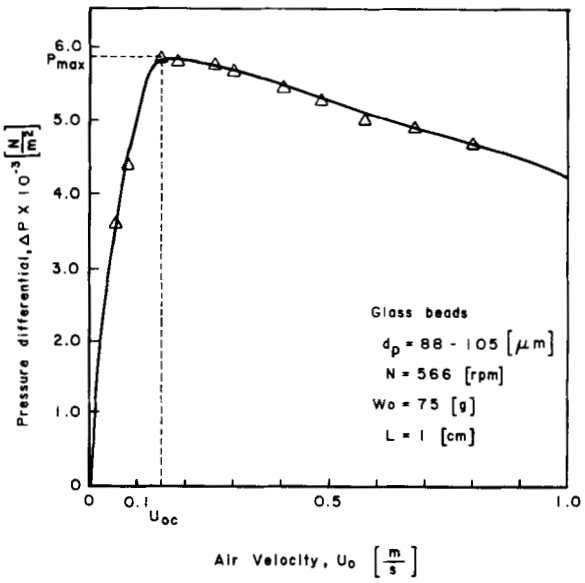

Figure 6. Pressure differential as a function of the superficial velocity of the fluidizing air.

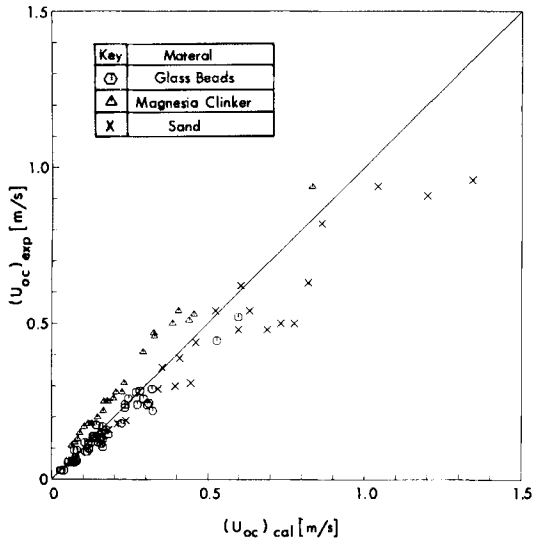

Figure 7. Comparison of the experimentally measured critical fluidizing velocities with the calculated values based on the present model.

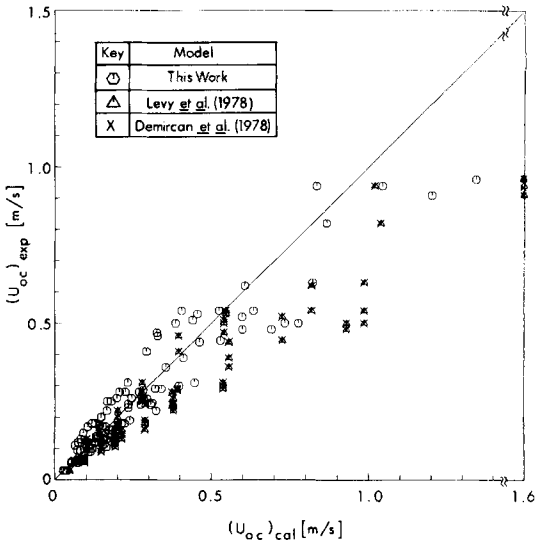

Figure 9. Comparison between the experimentally measured and calculated critical fluidizing velocities.

$$\frac{du_r}{dr} = 0 \tag{25}$$

and the term $\rho_f u_{oc}^2/r_o$ in Eq. 24 vanishes (see Eqs. A7 through A9). Furthermore, if the centrifugal force on the fluid is assumed negligible, Eq. 24 reduces to

$$\phi_1 u_{oc} + \phi_2 u_{oc}^2 = (1 - \epsilon)(\rho_s - \rho_f)\omega^2 r_o \tag{26}$$

This is the model proposed by Levy et al. (1978).

If the centrifugal acceleration, $\omega^2 r_o$, is replaced by the gravitational acceleration, g, Eq. 26 reduces to

$$\phi_1 u_{oc} + \phi_2 u_{oc}^2 = (1 - \epsilon)(\rho_s - \rho_f)g \tag{27}$$

This is the equation used for the columnar fluidized bed in the gravitational field.

EXPERIMENT

A schematic of the experimental apparatus is shown in Figure 3 and the sectional drawing of the apparatus is shown in Figures 4 and 5. The apparatus consisted of a cylindrical basket that rotated about a horizontal axis. The range of rotational speed of the basket was 400 ~ 800 rpm. Glass beads, magnesia clinker, and sand particles were fluidized; the characteristics of these particles are listed in Table 2. Air was used as the fluidized medium; its flow rate was measured by an orifice flow meter. The pressure differential was measured by a manometer, and the thickness of the fluidized bed was measured by a stroboscope.

A known weight of particles was loaded into the bed. After the rotational speed of the basket was established, injection of air into the bed was initiated, and the total pressure differentials were recorded at various air velocities. Experiments were also conducted without particles to obtain the pressure differentials across the distributor under the same operating conditions. The pressure differential through the fluidized bed was, then, calculated by subtracting the pressure differential across the distributor

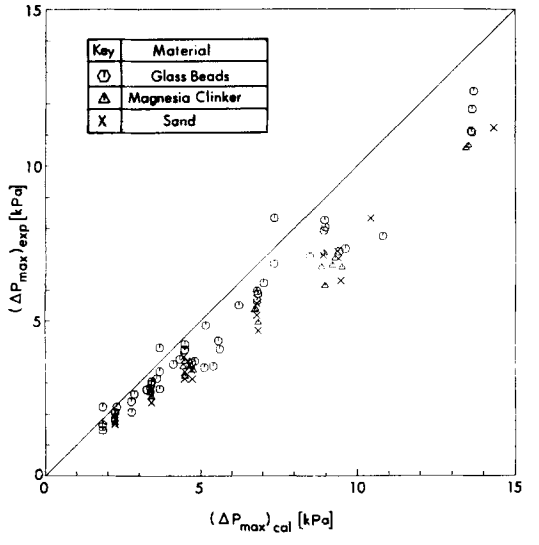

Figure 8. Comparison between the experimentally measured maximum pressure differentials with the calculated values based on the present model.

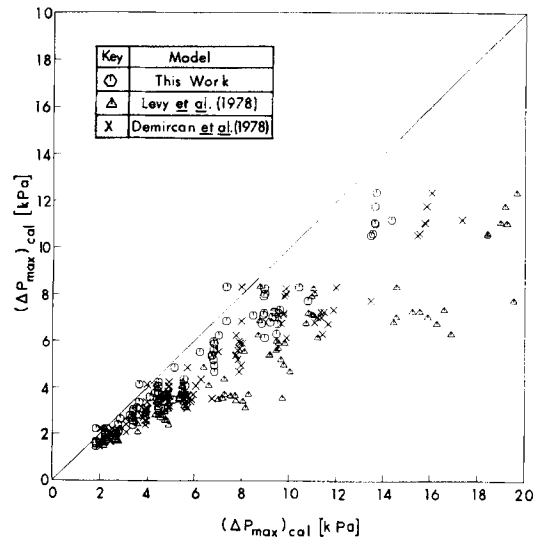

Figure 10. Comparison between the experimentally measured and calculated maximum pressure differentials.

from the total pressure differential. The critical fluidizing velocity, u_{oc}, and the maximum pressure differential, ΔP_{max}, were identified from the data. Experiments were repeated by changing the rotational speed of the basket.

The operating conditions and experimental data obtained are listed in Appendix B.

RESULTS AND DISCUSSION

The pressure differential as a function of the superficial velocity of the fluidizing air of a particular run is plotted in Figure 6. As shown in the figure, the pressure differential, ΔP, through the centrifugal fluidized bed increased as the superficial air velocity based on the outside surface area of the basket, u_o, was increased, and the pressure differential reached the maximum when the air velocity reached the critical fluidization velocity, u_{oc}. After the onset of fluidization, the pressure differential declined as the air velocity continuously increased.

Figures 7 and 8 compare the critical fluidization velocity, u_{oc}, calculated by Eq. 18 and the maximum pressure differential, ΔP_{max}, calculated by Eq. 22 with their respective experimentally measured data. The agreement between the calculated values and the experimental data is satisfactory, indicating that the present mechanistic model is valid and that the derived equations based on the model are of practical use.

The experimentally obtained values of the critical fluidizing velocity and maximum pressure differential are compared with the values estimated by the present model and two other available models (Demircan et al., 1978; Levy et al., 1978) in Figures 9 and 10, respectively (see also Appendix C). It appears that the agreement between the other two models with the experimental data is less satisfactory than that of the present model with the experimental data. It can be seen in Figure 9 that the critical fluidizing velocities predicated by the model of Demircan et al. (1978) are essentially the same as those predicted by the model of Levy et al. (1978). This indicates that the modified Wen-Yu correlation and the modified Ergun's equation yield about the same results. The deviations of these two models from the experimental data are attributable to the fact that the centrifugal force on the fluid and the curvature effect of a cylindrical bed are assumed negligible. The effects of these two contributions on the predicted maximum pressure differential are even more profound, as shown in Figure 10. The deviation of the model of Levy et al. (1978) is especially appreciable when the ratio of the radii of the outside and inside boundaries of the bed, r_o/r_i, is large. This arises from the fact that the effect of curvature is neglected in their model as discussed before.

The results indicate the characteristics of a centrifugal fluidized bed are substantially different from those of a gravitational fluidized bed. Therefore, the known hydrodynamic relations of the latter cannot be applied to the former. It is, therefore, highly desirable that additional hydrodynamic data, e.g., pressure drops, be obtained, especially in the region above incipient fluidization.

NOTATION

d_p = particle diameter, m
F = force exerted by the fluidizing medium on the particles in the centrifugal bed, N
F_d = drag force by viscous transfer, N
F_a = accelerated force on element, N
G = effective weight of particle in the bed, N
g_c = gravitational acceleration, m/s^2
L = width of the basket, m
M_s = mass of particles in the bed, kg
P = pressure, N/m^2
ΔP = pressure differential, N/m^2
ΔP_{max} = maximum pressure differential, N/m^2
r = radial coordinate, m
r_i = inside radius of the fluidized bed, m
r_o = outside radius of the fluidized bed, m
u, u_r = superficial fluid velocity in the packed bed, m/s
u_o = superficial fluid velocity based on the outside radius, m/s
u_{oc} = critical fluidizing velocity base on the outside radius, m/s

Greek Letters

ϵ = void fraction of the packed bed
μ = fluid viscosity, N·S/m^2
ρ_f = fluid density, kg/m^3
ρ_s = solid density, kg/m^3
ϕ_s = sphericity of the solid particles
ω = angular velocity, rad/s

LITERATURE CITED

Demircan, N., B. H. Gibbs, J. Swithenbank, and D. S. Taylor, "Rotating Fluidized Bed Combustor," in *Fluidization*, 270, Eds., J. F. Davidson and D. L. Keairns, Cambridge University Press, Cambridge, England (1978).

Ergun, S., "Fluid Flow Through Packed Column," *Chem. Eng. Prog.*, **48**, 89 (1952).

Fan, L. T., "Fluidized Bed Combustion in Centrifugal Field," *Energy Commun.*, **4**, 509 (1978).

Farkas, D. F., M. E. Lazar, and T. A. Butterworth, "The Centrifugal Fluidized Bed," *Food Technol.*, **23**, 125 (1969).

Gal, E., G. I. Tardos, and R. Pfeffer, "An Experimental Evaluation of the Rotating Fluidized Bed Filter," *World Filtration Congress III*, **1**, 78, Upland Press, Croydon, England (1982).

Gelperin, N. I., V. G. Ainshtein, and I. D. Goikhman, "Rate of Inception of Fluidization and Expansion of a Fluidized Layer in a Centrifugal Force Field," *Knim. Neft. Mash.*, 18 (1964).

Kroger, D. G., E. K. Levy, and J. C. Chen, "Flow Characteristics in Packed and Fluidized Rotating Beds," *Powder Technol.*, **24**, 9 (1979).

Kroger, D. G., G. Abdelnour, E. K. Levy, and J. Chen, "Centrifugal Fluidization: Effects of Particle Density and Size Distribution," *Chem. Eng. Commun.*, **5**, 55 (1980).

Lazar, M. E., and D. F. Farkas, "The Centrifugal Fluidized Bed. 2. Drying Studies on Piece-form Foods," *Food Sci.*, **36**, 315 (1971).

Levy, E., N. Martin, and J. Chen, "Minimum Fluidization and Startup of a Centrifugal Fluidized Bed," in *Fluidization*, 71, Ed., D. L. Kearins, Cambridge University Press, Cambridge (1978).

Takahashi, T., Z. Tanaka, and L. T. Fan, "Performance of a Rotating Fluidized Bed," *J. Chem. Eng. Japan*, **17**, No. 2 (1984).

Wen, C. Y., and Y. H. Yu, "A Generalized Method for Predicting the Minimum Fluidization Velocity," *Chem. Eng. Symp. Ser.*, **67**(62), 100 (1966).

Manuscript received Apr. 13, 1984; revision received June 19, and accepted July 3.

APPENDIX A: DERIVATION OF EQ. 1

Under a steady state flow condition, if the gravitational force is assumed to be negligible, the momentum balance around fluid in a small volumetric element in the packed bed situated in the centrifugal fields yields (see Figure 1)

$$\begin{bmatrix}\text{Rate of momentum}\\ \text{gain by convection}\end{bmatrix} + \begin{bmatrix}\text{Pressure force}\\ \text{on element}\end{bmatrix} + \begin{bmatrix}\text{Drag force by}\\ \text{viscous transfer}\end{bmatrix} + \begin{bmatrix}\text{Accelerational force}\\ \text{on element}\end{bmatrix} = 0 \quad \text{(A1)}$$

Assuming that the void fraction of fluid in the packed bed is constant, we have

$$[\epsilon(r\Delta\theta)Lu_r\rho_f u_r|_r - \epsilon(r\Delta\theta)Lu_r\rho_f u_r|_{r+\Delta r}] + \left[\epsilon(r\Delta\theta)Lp|_r - \epsilon(r\Delta\theta)LP|_{r+\Delta r} + 2\epsilon(\Delta r)L\sin\frac{(\Delta\theta)}{2}\cdot P|_{r+\Delta r/2}\right] + [\epsilon(\Delta\theta)L(\Delta r)F_d] + [\epsilon(r\Delta\theta)L(\Delta r)F_a] = 0 \quad \text{(A2)}$$

where F_d is the drag force exerted on the unit volume of fluid in the element by viscous transfer, and F_a is the accelerational force exerted on the unit volume of fluid in the element. The continuity of fluid gives

$$2\pi rL\epsilon u_r\rho_f = \text{constant}$$

or

$$ru_r\rho_f|_r = ru_r\rho_f|_{r+\Delta r}$$

Dividing both sides of Eq. A2 by the volume of fluid in the element, $\epsilon(r\Delta\theta)L(\Delta r)$, gives

$$\frac{\rho_f u_r}{\Delta r}[u_r|_r - u_r|_{r+\Delta r}] + \frac{1}{r\Delta r}[(Pr)|_r - (Pr)|_{r+\Delta r}] + \frac{2\sin\frac{(\Delta\theta)}{2}\cdot P|_{r+\Delta r/2}}{r\Delta\theta} + F_d + F_a = 0 \quad \text{(A3)}$$

As

$$(\Delta\theta)\to 0$$

$$\lim_{(\Delta\theta)\to 0}\frac{\sin\frac{(\Delta\theta)}{2}}{(\Delta\theta)} = \frac{1}{2}$$

and thus Eq. A3 can be rewritten as

$$\rho_f u_r\frac{u_r|_r - u_r|_{r+\Delta r}}{\Delta r} + \frac{1}{r}\frac{(Pr)|_r - (Pr)|_{r+\Delta r}}{\Delta r} + \frac{P|_{r+\Delta r/2}}{r} + F_d + F_a = 0 \quad \text{(A4)}$$

By letting

$$\Delta r\to 0$$

we obtain

$$-\rho_f u_r\frac{du_r}{dr} - \frac{1}{r}\frac{d(Pr)}{dr} + \frac{P}{r} + F_d + F_a = 0 \quad \text{(A5)}$$

Rearranging the equation yields

$$-\rho_f u_r\frac{du_r}{dr} - \frac{dP}{dr} + F_d + F_a = 0 \quad \text{(A6)}$$

According to Ergun (1952), the drag force exerted on the unit volume of fluid by viscous transfer in the packed bed can be expressed semiempirically as

$$F_d = \phi_1|u_r| + \phi_2|u_r|^2$$

where ϕ_1 and ϕ_2 are defined, respectively, as

$$\phi_1 = \frac{150(1-\epsilon)^2\mu}{\epsilon^3(\phi_s d_p)^2}$$

$$\phi_2 = \frac{1.75(1-\epsilon)\rho_f}{\epsilon^3\phi_s d_p}$$

The accelerational force exerted on the unit volume of fluid is

$$F_a = \rho_f\omega^2 r$$

when the fluid flows through the centrifugal field with a rotational speed of ω, provided that the gravitational effect is negligible. Thus Eq. A6 can be rewritten as

$$\frac{dP}{dr} = \phi_1|u_r| + \phi_2|u_r|^2 + \rho_f\omega^2 r - \rho_f u_r\frac{du_r}{dr} \quad \text{(A7)}$$

The continuity equation of fluid gives

$$u_r r = u_o r_o \quad \text{or} \quad \frac{du_r}{dr} = -\frac{u_o r_o}{r^2} = -\frac{u_r}{r} \quad \text{(A8)}$$

Substituting Eq. A8 into Eq. A7 yields

$$\left.\begin{aligned}\frac{dP}{dr} &= \phi_1|u_r| + \phi_2|u_r|^2 + \rho_f\omega^2 r + \rho_f\frac{u_r^2}{r}\\ \text{or}\\ \frac{dP}{dr} &= \phi_1|u_r| + \left(\phi_2 + \frac{\rho_f}{r}\right)|u_r|^2 + \rho_f\omega^2 r\end{aligned}\right\} \quad \text{(A9)}$$

This is Eq. 1 in the text.

Appendix B: Table of Operating Conditions and Experimental Results

Run No.*	d_p, μm	M_s, kg	N, rpm	r_i, m	ρ_s, kg/m³	ϵ	u_{oc}, m/s	ΔP_{max}, kPa
GP-1-1	68.5	0.100	400	0.0598	2,410	0.463	0.030	1.67
GP-1-2	68.5	0.100	566	0.0598	2,410	0.463	0.060	3.37
GP-1-3	68.5	0.100	800	0.0598	2,410	0.463	0.150	6.84
GP-2-1	96.5	0.100	400	0.0606	2,450	0.440	0.060	1.59
GP-2-2	96.5	0.100	500	0.0606	2,450	0.440	0.120	2.65
GP-2-3	96.5	0.100	600	0.0606	2,450	0.440	0.145	3.60
GP-2-4	96.5	0.100	700	0.0606	2,450	0.440	0.260	4.08
GP-3-1	96.5	0.125	400	0.0574	2,450	0.440	0.070	2.23
GP-3-2	96.5	0.125	500	0.0574	2,450	0.440	0.100	3.14
GP-3-3	96.5	0.125	600	0.0574	2,450	0.440	0.160	4.85
GP-3-4	96.5	0.125	700	0.0574	2,450	0.440	0.240	6.22
GP-4-1	96.5	0.150	400	0.0540	2,450	0.440	0.055	2.41
GP-4-2	96.5	0.150	500	0.0540	2,450	0.440	0.090	3.76
GP-4-3	96.5	0.150	600	0.0540	2,450	0.440	0.130	5.51
GP-4-4	96.5	0.150	700	0.0540	2,450	0.440	0.180	7.08

Run No. *	d_p, μm	M_s, kg	N, rpm	r_i, m	ρ_s, kg/m^3	ϵ	u_{oc}, m/s	ΔP_{max}, kPa
GP-5-1	96.5	0.175	400	0.0503	2,450	0.440	0.060	2.79
GP-5-2	96.5	0.175	500	0.0503	2,450	0.440	0.090	3.49
GP-6-1	137.0	0.100	400	0.0607	2,490	0.441	0.105	1.48
GP-6-2	137.0	0.100	566	0.0607	2,490	0.441	0.220	2.81
GP-7-1	137.0	0.150	400	0.0542	2,490	0.441	0.120	2.07
GP-7-2	137.0	0.150	566	0.0542	2,490	0.441	0.260	4.35
GP-8-1	68.5	0.050	400	0.0598	2,410	0.463	0.030	2.23
GP-8-2	68.5	0.050	566	0.0598	2,410	0.463	0.060	4.13
GP-8-3	68.5	0.050	800	0.0598	2,410	0.463	0.135	8.32
GP-9-1	68.5	0.075	400	0.0475	2,410	0.463	0.030	3.06
GP-9-2	68.5	0.075	566	0.0475	2,410	0.463	0.060	5.87
GP-9-3	68.5	0.075	800	0.0475	2,410	0.463	0.140	12.35
GP-10-1	68.5	0.100	400	0.0357	2,410	0.463	0.030	3.70
GP-10-2	68.5	0.100	566	0.0357	2,410	0.463	0.060	7.32
GP-11-1	96.5	0.050	400	0.0578	2,450	0.440	0.065	2.07
GP-11-2	96.5	0.050	566	0.0578	2,450	0.440	0.130	4.07
GP-11-3	96.5	0.050	800	0.0578	2,450	0.440	0.240	8.25
GP-12-1	96.5	0.075	400	0.0492	2,450	0.440	0.063	2.96
GP-12-2	96.5	0.075	566	0.0492	2,450	0.440	0.140	5.88
GP-12-3	96.5	0.075	800	0.0492	2,450	0.440	0.280	11.78
GP-13-1	96.5	0.100	400	0.0332	2,450	0.440	0.055	3.53
GP-13-2	96.5	0.100	566	0.0332	2,450	0.440	0.120	7.72
GP-14-1	137.0	0.050	400	0.0580	2,490	0.441	0.115	2.05
GP-14-2	137.0	0.050	566	0.0580	2,490	0.441	0.245	4.24
GP-14-3	137.0	0.050	800	0.0580	2,490	0.441	0.520	8.02
GP-15-1	137.0	0.075	400	0.0496	2,490	0.441	0.135	2.94
GP-15-2	137.0	0.075	566	0.0496	2,490	0.441	0.240	5.65
GP-15-3	137.0	0.075	800	0.0496	2,490	0.441	0.445	11.04
GP-16-1	137.0	0.100	400	0.0394	2,490	0.441	0.115	3.65
GP-16-2	137.0	0.100	566	0.0394	2,490	0.441	0.230	7.24
GP-17-1	99.5	0.050	400	0.0581	2,410	0.421	0.095	2.04
GP-17-2	99.5	0.050	566	0.0581	2,410	0.421	0.170	4.04
GP-17-3	99.5	0.050	800	0.0581	2,410	0.421	0.290	7.91
GP-18-1	99.5	0.075	400	0.0497	2,410	0.421	0.095	3.04
GP-18-2	99.5	0.075	566	0.0497	2,410	0.421	0.175	5.96
GP-18-3	99.5	0.075	800	0.0497	2,410	0.421	0.285	11.08
MP-1-1	96.5	0.050	400	0.0589	3,630	0.598	0.180	1.84
MP-1-2	96.5	0.050	566	0.0589	3,630	0.598	0.310	3.52
MP-1-3	96.5	0.050	800	0.0589	3,630	0.598	0.530	6.73
MP-2-1	96.5	0.075	400	0.0511	3,630	0.598	0.170	2.69
MP-2-2	96.5	0.075	566	0.0511	3,630	0.598	0.280	5.35
MP-2-3	96.5	0.075	800	0.0511	3,630	0.598	0.540	10.53
MP-3-1	96.5	0.100	400	0.0420	3,630	0.598	0.150	3.54
MP-3-2	96.5	0.100	566	0.0420	3,630	0.598	0.250	6.78
MP-4-1	137.0	0.050	400	0.0574	3,620	0.630	0.280	1.73
MP-4-2	137.0	0.050	566	0.0574	3,620	0.630	0.510	3.21
MP-4-3	137.0	0.050	800	0.0574	3,620	0.630	0.940	6.12
MP-5-1	137.0	0.075	400	0.0485	3,620	0.630	0.260	2.56
MP-5-2	137.0	0.075	566	0.0485	3,620	0.630	0.500	4.94
MP-6-1	137.0	0.100	400	0.0376	3,620	0.630	0.250	3.41
MP-6-2	137.0	0.100	566	0.0376	3,620	0.630	0.470	6.72
MP-7-1	81.0	0.050	400	0.0589	3,650	0.596	0.130	1.94
MP-7-2	81.0	0.050	566	0.0589	3,650	0.596	0.220	3.69
MP-7-3	81.0	0.050	800	0.0589	3,650	0.596	0.460	7.18
MP-8-1	81.0	0.075	400	0.0512	3,650	0.596	0.120	2.79
MP-8-2	81.0	0.075	566	0.0512	3,650	0.596	0.200	5.38
MP-8-3	81.0	0.075	800	0.0512	3,650	0.596	0.410	10.61
MP-9-1	81.0	0.100	400	0.0420	3,650	0.596	0.110	3.70
MP-9-2	81.0	0.100	566	0.0420	3,650	0.596	0.180	7.01
SP-1-1	230.0	0.050	400	0.0584	2,670	0.466	0.310	1.71
SP-1-2	230.0	0.050	566	0.0584	2,670	0.466	0.630	3.36
SP-2-1	230.0	0.075	400	0.0503	2,670	0.466	0.300	2.58
SP-2-2	230.0	0.075	566	0.0503	2,670	0.466	0.500	5.18
SP-3-1	230.0	0.100	400	0.0405	2,670	0.466	0.290	3.42
SP-3-2	230.0	0.100	566	0.0405	2,670	0.466	0.540	7.00
SP-4-1	163.0	0.050	400	0.0586	2,670	0.461	0.190	1.95
SP-4-2	163.0	0.050	566	0.0586	2,670	0.461	0.440	3.84
SP-4-3	163.0	0.050	800	0.0586	2,670	0.461	0.820	7.11

Run No.*	d_p, μm	M_s, kg	N, rpm	r_t, m	ρ_s, kg/m³	ϵ	u_{oc}, m/s	ΔP_{max}, kPa
SP-5-1	163.0	0.075	400	0.0505	2,670	0.461	0.180	2.78
SP-5-2	163.0	0.075	566	0.0505	2,670	0.461	0.390	5.57
SP-5-3	163.0	0.075	700	0.0505	2,670	0.461	0.620	8.30
SP-6-1	163.0	0.100	400	0.0409	2,670	0.461	0.160	3.63
SP-6-2	163.0	0.100	566	0.0409	2,670	0.461	0.360	7.24
SP-6-3	163.0	0.100	700	0.0409	2,670	0.461	0.540	11.19
SP-7-1	323.5	0.050	400	0.0583	2,700	0.476	0.500	1.66
SP-7-2	323.5	0.050	566	0.0583	2,700	0.476	0.960	3.13
SP-8-1	323.5	0.075	400	0.0500	2,700	0.476	0.480	2.38
SP-8-2	323.5	0.075	566	0.0500	2,700	0.476	0.910	4.67
SP-9-1	323.5	0.100	400	0.0401	2,700	0.476	0.480	3.12
SP-9-2	323.5	0.100	566	0.0401	2,700	0.476	0.940	6.28

* Materials used for run number: GP, glass bead; MP, magnesia clinker; SP, sand.

Appendix C: Table of Comparison of Experimentally Measured and Calculated Critical Fluidizing Velocity and Maximum Pressure Drop

Run No.*	Critical Fluidizing Velocity, m/s				Maximum Pressure Drop, kPa			
	Exp.	(1)*	(2)*	(3)*	Exp.	(1)*	(2)*	(3)*
GP-1-1	0.030	0.040	0.048	0.048	1.67	1.84	2.19	2.00
GP-1-2	0.060	0.080	0.096	0.096	3.37	3.67	4.38	4.00
GP-1-3	0.150	0.160	0.190	0.190	6.84	7.34	8.75	7.98
GP-2-1	0.060	0.082	0.096	0.096	1.59	1.83	2.15	1.98
GP-2-2	0.120	0.127	0.150	0.149	2.65	2.86	3.37	3.09
GP-2-3	0.145	0.182	0.214	0.214	3.60	4.11	4.85	4.45
GP-2-4	0.260	0.246	0.289	0.289	4.08	5.60	6.60	6.05
GP-3-1	0.070	0.078	0.096	0.096	2.23	2.29	2.83	2.53
GP-3-2	0.100	0.121	0.150	0.149	3.14	3.58	4.43	3.96
GP-3-3	0.160	0.174	0.214	0.214	4.85	5.16	6.38	5.70
GP-3-4	0.240	0.235	0.289	0.289	6.22	7.02	8.69	7.75
GP-4-1	0.055	0.074	0.096	0.096	2.41	2.77	3.60	3.12
GP-4-2	0.090	0.115	0.150	0.149	3.76	4.32	5.62	4.88
GP-4-3	0.130	0.165	0.214	0.214	5.51	6.22	8.10	7.02
GP-4-4	0.180	0.223	0.289	0.289	7.08	8.47	11.04	9.56
GP-5-1	0.060	0.070	0.096	0.096	2.79	3.26	4.48	3.76
GP-5-2	0.090	0.109	0.150	0.149	3.49	5.10	7.01	5.88
GP-6-1	0.105	0.165	0.194	0.193	1.48	1.84	2.17	1.99
GP-6-2	0.220	0.323	0.379	0.378	2.81	3.68	4.35	3.98
GP-7-1	0.120	0.150	0.194	0.193	2.07	2.78	3.61	3.13
GP-7-2	0.260	0.294	0.379	0.378	4.35	5.56	7.25	6.27
GP-8-1	0.030	0.040	0.048	0.048	2.23	1.84	2.19	2.00
GP-8-2	0.060	0.080	0.096	0.096	4.13	3.67	4.38	4.00
GP-8-3	0.135	0.160	0.190	0.190	8.32	7.34	8.75	7.98
GP-9-1	0.030	0.033	0.048	0.048	3.06	3.42	4.90	4.01
GP-9-2	0.060	0.067	0.096	0.096	5.87	6.84	9.82	8.02
GP-9-3	0.140	0.133	0.190	0.190	12.35	13.67	19.64	16.03
GP-10-1	0.030	0.028	0.048	0.048	3.70	4.79	8.27	5.94
GP-10-2	0.060	0.056	0.096	0.096	7.32	9.60	16.58	11.89
GP-11-1	0.065	0.078	0.096	0.096	2.07	2.24	2.74	2.46
GP-11-2	0.130	0.156	0.191	0.191	4.07	4.48	5.50	4.93
GP-11-3	0.240	0.306	0.375	0.374	8.25	8.94	11.01	9.85
GP-12-1	0.063	0.069	0.096	0.096	2.96	3.40	4.76	3.95
GP-12-2	0.140	0.137	0.191	0.191	5.88	6.82	9.55	7.92
GP-12-3	0.280	0.270	0.375	0.374	11.78	13.62	19.15	15.81
GP-13-1	0.055	0.054	0.096	0.096	3.53	5.39	9.70	6.73
GP-13-2	0.120	0.107	0.191	0.191	7.72	10.79	19.52	13.47
GP-14-1	0.115	0.159	0.194	0.193	2.05	2.24	2.75	2.46
GP-14-2	0.245	0.311	0.379	0.378	4.24	4.48	5.51	4.93
GP-14-3	0.520	0.597	0.725	0.724	8.02	8.96	11.06	9.85
GP-15-1	0.135	0.140	0.194	0.193	2.94	3.40	4.74	3.94
GP-15-2	0.240	0.275	0.379	0.378	5.65	6.81	9.54	7.89
GP-15-3	0.445	0.528	0.725	0.724	11.04	13.62	19.23	15.76

Run No.*	Critical Fluidizing Velocity, m/s				Maximum Pressure Drop, kPa			
	Exp.	(1)*	(2)*	(3)*	Exp.	(1)*	(2)*	(3)*
GP-16-1	0.115	0.120	0.194	0.193	3.65	4.70	7.70	5.73
GP-16-2	0.230	0.235	0.379	0.378	7.24	9.41	15.56	11.48
GP-17-1	0.095	0.082	0.101	0.100	2.04	2.23	2.73	2.45
GP-17-2	0.170	0.163	0.199	0.199	4.04	4.46	5.46	4.91
GP-17-3	0.290	0.321	0.391	0.391	7.91	8.92	10.94	9.80
GP-18-1	0.095	0.073	0.101	0.100	3.04	3.40	4.71	3.93
GP-18-2	0.175	0.144	0.199	0.199	5.96	6.80	9.46	7.87
GP-18-3	0.285	0.283	0.391	0.391	11.08	13.59	18.96	15.73
MP-1-1	0.180	0.118	0.142	0.142	1.84	2.21	2.67	2.42
MP-1-2	0.310	0.233	0.280	0.280	3.52	4.42	5.35	4.84
MP-1-3	0.530	0.455	0.547	0.546	6.73	8.84	10.72	9.66
MP-2-1	0.170	0.105	0.142	0.142	2.69	3.36	4.56	3.85
MP-2-2	0.280	0.207	0.280	0.280	5.35	6.72	9.16	7.72
MP-2-3	0.540	0.406	0.547	0.546	10.53	13.43	18.38	15.42
MP-3-1	0.150	0.091	0.142	0.142	3.54	4.59	7.18	5.53
MP-3-2	0.250	0.180	0.280	0.280	6.78	9.19	14.44	11.08
MP-4-1	0.280	0.226	0.279	0.278	1.73	2.24	2.77	2.47
MP-4-2	0.510	0.440	0.540	0.539	3.21	4.48	5.57	4.95
MP-4-3	0.940	0.833	1.018	1.017	6.12	8.96	11.21	9.89
MP-5-1	0.260	0.198	0.279	0.278	2.56	3.41	4.85	3.98
MP-5-2	0.500	0.386	0.540	0.539	4.94	6.84	9.78	7.97
MP-6-1	0.250	0.168	0.279	0.278	3.41	4.74	8.03	5.82
MP-6-2	0.470	0.326	0.540	0.539	6.72	9.50	16.28	11.66
MP-7-1	0.130	0.084	0.101	0.101	1.94	2.23	2.70	2.44
MP-7-2	0.220	0.166	0.201	0.200	3.69	4.47	5.40	4.89
MP-7-3	0.460	0.328	0.395	0.395	7.18	8.93	10.81	9.77
MP-8-1	0.120	0.075	0.101	0.101	2.79	3.38	4.58	3.88
MP-8-2	0.200	0.148	0.201	0.200	5.38	6.76	9.18	7.76
MP-8-3	0.410	0.293	0.395	0.395	10.61	13.51	18.40	15.51
MP-9-1	0.110	0.065	0.101	0.101	3.70	4.63	7.25	5.59
MP-9-2	0.180	0.129	0.201	0.200	7.01	9.28	14.55	11.20
SP-1-1	0.310	0.445	0.536	0.536	1.71	2.23	2.75	2.45
SP-1-2	0.630	0.821	0.985	0.984	3.36	4.47	5.55	4.91
SP-2-1	0.300	0.396	0.536	0.536	2.58	3.39	4.75	3.91
SP-2-2	0.500	0.733	0.985	0.984	5.18	6.80	9.65	7.83
SP-3-1	0.290	0.341	0.536	0.536	3.42	4.68	7.74	5.68
SP-3-2	0.540	0.634	0.985	0.984	7.00	9.39	15.89	11.36
SP-4-1	0.190	0.239	0.289	0.288	1.95	2.22	2.71	2.44
SP-4-2	0.440	0.461	0.555	0.554	3.84	4.45	5.45	4.88
SP-4-3	0.820	0.864	1.037	1.035	7.11	8.90	10.95	9.75
SP-5-1	0.180	0.212	0.289	0.288	2.78	3.39	4.68	3.91
SP-5-2	0.390	0.410	0.555	0.554	5.57	6.80	9.45	7.83
SP-5-3	0.620	0.606	0.818	0.817	8.30	10.40	14.55	11.98
SP-6-1	0.160	0.183	0.289	0.288	3.63	4.67	7.51	5.66
SP-6-2	0.360	0.354	0.555	0.554	7.24	9.35	15.24	11.33
SP-6-3	0.540	0.525	0.818	0.817	11.19	14.32	23.57	17.32
SP-7-1	0.500	0.776	0.930	0.929	1.66	2.23	2.79	2.45
SP-7-2	0.960	1.344	1.600	1.599	3.13	4.47	5.64	4.90
SP-8-1	0.480	0.691	0.930	0.929	2.38	3.41	4.91	3.93
SP-8-2	0.910	1.201	1.600	1.599	4.67	6.84	10.05	7.88
SP-9-1	0.480	0.598	0.930	0.929	3.12	4.71	8.14	5.70
SP-9-2	0.940	1.043	1.600	1.599	6.28	9.46	16.90	11.42

* (1) Predicted in this work.
* (2) Predicted by the model of Levy et al. (1978).
* (3) Predicted by the model of Demircan et al. (1978).